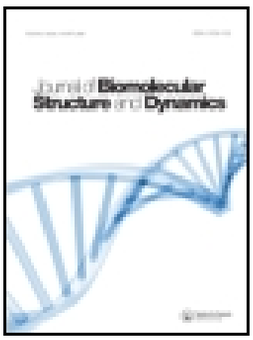

Taylor & Francis
Taylor & Francis Group

Journal of Biomolecular Structure and Dynamics

ISSN: 0739-1102 (Print) 1538-0254 (Online) Journal homepage: https://www.tandfonline.com/loi/tbsd20

Ruthenium complexes with *mono*- or *bis*-heterocyclic chelates: DNA/BSA binding, Antioxidant and Anticancer studies

Sanam Maikoo, Abir Chakraborty, Nyeleti Vukea, Laura Margaret Kirkpatrick Dingle, William John Samson, Jo-Anne de la Mare, Adrienne Lesley Edkins & Irvin Noel Booysen

To cite this article: Sanam Maikoo, Abir Chakraborty, Nyeleti Vukea, Laura Margaret Kirkpatrick Dingle, William John Samson, Jo-Anne de la Mare, Adrienne Lesley Edkins & Irvin Noel Booysen (2020): Ruthenium complexes with *mono*- or *bis*-heterocyclic chelates: DNA/BSA binding, Antioxidant and Anticancer studies, Journal of Biomolecular Structure and Dynamics, DOI: 10.1080/07391102.2020.1775126

To link to this article: https://doi.org/10.1080/07391102.2020.1775126

Ruthenium complexes with *mono*- or *bis*-heterocyclic chelates: DNA/BSA binding, Antioxidant and Anticancer studies

Sanam Maikoo[a], Abir Chakraborty[b], Nyeleti Vukea[b], Laura Margaret Kirkpatrick Dingle[b], William John Samson[b], Jo-Anne de la Mare[b], Adrienne Lesley Edkins[b], Irvin Noel Booysen*[a]

[a]School of Chemistry and Physics, University of KwaZulu-Natal, Pietermaritzburg, South Africa

[b]Biomedical Biotechnology Research Unit, Department of Biochemistry and Microbiology, Rhodes University, Grahamstown, South Africa

*Corresponding author: E-mail: Booyseni@ukzn.ac.za

Abstract

Deoxyribonucleic acid (DNA) and bovine serum albumin (BSA) binding interactions for a series of ruthenium heterocyclic complexes were monitored using ultraviolet-visible (UV-Vis) spectrophotometry, fluorescence emission spectroscopy and agarose gel electrophoresis. Investigations of the DNA interactions for the metal complexes revealed that they are groove-binders with intrinsic binding constants in the order of 10^4 – 10^7 M^{-1}. Electronic spectrophotometric DNA titrations of the *bis*-heterocyclic metal complexes illustrated hypochromism of their intraligand electronic transitions and the presence of diffuse isosbestic points which are synonymous with homogeneous binding modes. Metal complexes with the *mono*-heterocyclic chelates also showed alterations in their intraligand transitions and changes in their metal-based electronic transitions which are suggestive of metal coordination to the CT-DNA structure. Using agarose gel electrophoresis assessments, Hoechst DNA binding competition studies corroborate that the metal complexes are DNA groove-binders. Optimal uptake of these metal complexes by BSA was observed based on their optimal apparent association and Stern-Volmer constants (K_{app} and K_{SV} > 10^4 M^{-1}). Radical scavenging studies revealed that the metal complexes have high activities towards the neutralization of NO and DPPH radicals. Data attained from the BSA electronic spectrophotometric titrations for the

majority of the metal complexes illustrated distinct hyperchromism accompanied with blue shifts which indicates unwinding of the protein strands. Predominately, the metal complexes showed moderate cytotoxicity against both triple-negative breast cancer and cervical cancer cell lines that was greater than that of 5-fluorouracil.

Keywords: Ruthenium heterocyclic complexes, DNA/BSA binding, antioxidant activities, cytotoxicity.

1. Introduction

Ruthenium-based anticancer drugs have demonstrated cytotoxicity against a wide variety of cancer cells accompanied with minimal side effects to healthy cells (Lazarević, Rilak, & Bugarčić Ž, 2017; Thota, Rodrigues, Crans, & Barreiro, 2018; Zhang & Sadler, 2017). It is hypothesized that the biocompatibility of these potential metallopharmaceuticals culminates from the similar chemistry of ruthenium and the essential metal, iron, as these elements are group congeners (Merlino, 2016). In addition, ruthenium can induce cancer cell apoptosis through utilization of its high coordination affinities to nucleotides (Pages, Ang, Wright, & Aldrich-Wright, 2015). Alteration of the co-ligands within the coordination sphere of ruthenium have been shown to lead to intriguing structure-activity relationships and diverse mechanisms of action (Zeng et al., 2017). In fact, the leading candidates of ruthenium chemotherapeutic agents, *e.g. trans*-[$RuCl_4$(DMSO)(Im)](ImH) (ImH = protonated imidazole) (NAMI-A), are pro-drugs which are activated upon hydrolysis (Dwyer, Johnson, Cazares, McFarlane Holman, & Kirk, 2018). Furthermore, conjugated aromatic chelating ligands of metal complexes are able to promote DNA interaction through intercalation or groove-binding as the possible mechanism of anticancer activity (Levina, Mitra, & Lay, 2009).

Current research focuses on designing target-specific ruthenium anticancer drugs and involves encompassing biologically relevant moieties (BAMs) in ligand scaffolds where the meticulously selected BAMs may facilitate defined biodistribution patterns (Caruso et al., 2016). This design approach is exemplified by arene metal complexes with flavone or chromone analogs, where a correlation between the lipophilicity and the *in vitro* screening of melanoma cell lines was found (Pastuszko, Majchrzak, Czyz, Kupcewicz, & Budzisz, 2016). In addition, a fascinating bifunctional metal complex, (ethacrynic acid-*g6*-benzylamide)(1,3,5-triaza-7-

phosphaadamantane)dichloride (ethaRAPTA) induced death of MCF-7 breast cancer cells, which is regarded as a significant advancement considering that these cells are resistant to cisplatin (Chatterjee, Biondi, Dyson, & Bhattacharyya, 2011). The dual functionality of this metal complex stems from the inherent cytotoxicity of the RAPTA constituent and ethacrynic acid-*g6*-benzylamide moiety's glutathione *S*-transferase inhibiting capability which combats drug resistance.

Heterocyclics such as benz(imidazole/othiazole) moieties are common to various organopharmaceuticals and their derivatives have been shown to exhibit *in vivo* therapeutic activities to common human cancers (Taha et al., 2015; Yadav & Ganguly, 2015; Yamin & Teplow, 2017). Moreover, metal-ligand synergistic correlations have been observed where the metal complexes have shown higher activities than their corresponding benz(imidazole/othiazole)-derived free-ligands. This phenomena is illustrated by the antimicrobial bioassays conducted on the metal complex, $[Ni_3(abb)_3(H_2O)_3(\mu\text{-ttc})](ClO_4)_3\cdot 3H_2O\cdot EtOH$ and its free-ligand, 1-(1*H*-benzimidazol-2-yl)-*N*-(1*H*-benzimidazol-2-ylmethyl)methanamine (abb) which showed that the metal complex displayed higher antimicrobial activity than the free-ligand (Kopel et al., 2015). In fact, complementary biological and anticancer activities of metal-based chemotherapeutic drugs can improve their efficacy by negating the common side-effects associated with secondary infections (Ng, Wu, & Aldrich-Wright, 2018).

In this research study, we report the synthesis and characterization of new metal complexes bearing *bis*-heterocyclic ligands as well as exploring the structure-activity correlations of the aforementioned metal complexes and those with mono-heterocyclic chelates, $[RuCl(Hobz)_2(PPh_3)]Cl$ (**3**) (Hobz = 2-hydroxyphenylbenzimidazole) and $[Ru^{III}Cl(obs)_2(PPh_3)]$ (**4**) (Hobs = 2-hydroxyphenylbenzothiazole). Two novel diamagnetic metal complexes, *cis*-$[Ru^{II}Cl(PPh_3)_2(ombb)](PF_6)$ (**1**) and *trans*-$[Ru^{II}Cl_2(PPh_3)_2$ (bbb)] (**2**) were synthesized from the reactions of *trans*-$[RuCl_2(PPh_3)_3]$ with *bis*-benzimidazole ligands, 2,2'-[oxy*bis*(methylene)]-*bis*-(1*H*-benzimidazole) (ombb) and 4,4'-*bis*(1*H*-benzimidazol-2-yl)-2,2'-bipyridine (bbb), respectively. The DNA and BSA interaction, antioxidant capabilities and *in vitro* anticancer activities of the metal complexes **1** – **4** were evaluated.

2. Experimental

2.1 Materials and methods

The metal precursor, *trans*-[$RuCl_2(PPh_3)_3$] and ammonium hexafluorophosphate as well as the organic precursors, including diglycolic acid, 2,2'-bipyridine-4,4'-dicarboxylic acid, *o*-phenylenediamine, were all procured from Sigma-Aldrich. High purity ascorbic acid, 2,2-diphenyl-1-picrylhydrazyl (DPPH), Griess reagent, sodium nitroprusside, phosphate buffered saline tablets (PBS), calf thymus (CT)-DNA, Bovine Serum Albumin (BSA) and electrochemical analysis grade tetrabutylammonium hexafluorophosphate were also obtained from Sigma Aldrich. Organic solvents were purchased from Merck SA and used without additional purification. The *bis*-benzimidazoles, ombb and bbb, as well as the *mono*-heterocyclic metal complexes **3** and **4,** were prepared according to literature trends (Adebisi, Booysen, Akerman, & Xulu, 2016; Swarnalatha, Rathnamala, Babu, & Bhuvanesh, 2016; Tavman & Çinarli, 2014). The synthetic procedures of **1** and **2** are described in the accompanying supporting information document.

^{31}P, ^{1}H and ^{13}C NMR spectra were obtained in DMSO-d_6 using a Bruker Advance 400 MHz spectrometer equipped with an autosampler. Solid-state infrared spectra were recorded using a Perkin-Elmer Spectrum 100 while electronic spectra were collected using a Perkin-Elmer Lambda 25. Melting point ranges were determined with the aid of a Stuart SMP3 melting point apparatus. Redox properties of the novel metal complexes **1** and **2** were probed using a Metrohm Autolab potentiostat in conjunction with a three electrode system: a glassy carbon working electrode (GCWE), a pseudo Ag|AgCl reference electrode and an auxiliary Pt counter electrode. Electrochemical grade tetrabutylammonium hexafluorophosphate (0.1 M) was added to the 2 mM dichloromethane solutions of the metal complexes as a supporting electrolyte. Fluorescence measurements were carried out using a 1 cm quartz emission cell and a Perkin Elmer LS-45 fluorescence spectrometer equipped with a xenon lamp source. Elemental analysis data were obtained using a CHNS-O Flash 2000 Organic Elemental Analyzer.

2.2 UV-Vis spectrophotometric DNA titrations and agarose gel electrophoresis assessment of DNA binding

The CT-DNA interaction studies of the metal complexes were performed at a pH of 7.2 in phosphate-buffered saline (PBS). The CT-DNA solution in PBS gave rise to a ratio of 1.9:1 at 260 nm and 280 nm, which implies that the CT-DNA was sufficiently free of protein. Using the molar absorption coefficient (ε_{260} = 6600 $M^{-1}cm^{-1}$), the CT-DNA concentration per nucleotide was calculated (Reichmann, Rice, Thomas, & Doty, 1954). The final CT-DNA stock solution was kept at 4 ºC and used within 2 days. Solutions of the metal complexes and CT-DNA were incubated at 25 ºC for 24 hours preceding any UV-Vis measurements [21]. Subsequently, UV-Vis spectra were collected of standard solutions for the respective metal complexes in DMSO and after the addition of varying concentrations of CT-DNA in PBS buffer. The intrinsic binding constant (K_b) was obtained by fitting the data obtained from the titration into the following equation:

$$\frac{[DNA]}{(\varepsilon_a - \varepsilon_b)} = \frac{[DNA]}{(\varepsilon_b - \varepsilon_f)} + \frac{1}{K_b(\varepsilon_a - \varepsilon_f)} \qquad \text{(A)}$$

In the above equation, [DNA] is the concentration of DNA in base pairs, ε_a is the extinction coefficient of the detected absorption band at the given DNA concentration [corresponding to A_{obs}/(complex)], ε_f is the extinction coefficient of the free metal complex in solution, and ε_b is the extinction coefficient of the fully bound metal complex to DNA. A slope of $1/(\varepsilon_a - \varepsilon_f)$ and Y intercept of $1/K_b(\varepsilon_b - \varepsilon_f)$ was found from a plot of [DNA]/(εa – εf) versus [DNA]. The ratio of the slope to the intercept is estimated to be the intrinsic binding constant (K_b) (Kaplanis et al., 2014).

In addition, the ability of metal complexes to interact with human genomic DNA (gDNA) isolated from cancer cell lines was assessed by agarose gel electrophoresis. Metal complexes at two different concentrations (50 µM and 200 µM, selected in relation to the IC_{50} values) or the vehicle control (DMSO) were incubated with 100 ng of gDNA in a total reaction volume of 20 μL. Reaction mixtures were incubated at 37°C for 2-4 hours, followed by electrophoresis for 1 hour at 90V in 1x Tris-acetic acid EDTA (TAE) buffer using 0.8% (w/v) agarose containing 0.5 μg/mL EtBr. The DNA was visualized under UV light. The assay was conducted as independent triplicates and the average fluorescence intensity of DNA treated with metal complexes was determined by ImageJ relative to the DMSO control.

The abilities of the metal complexes to compete with Hoechst for binding to DNA were assessed. Three concentrations of the metal complexes (5 µM, 50 µM and 100 µM) were incubated with a final concentration of 1 μg/mL of Hoechst-33342 in the presence or absence of DNA in a 100 μL reaction volume in a black-walled clear bottom 96 well plate at 25 °C. The fluorescence emission over the range of 400-600 nm was collected after excitation at 350 nm.

2.3 Antioxidant studies

Experimental methodologies for the radical scavenging measurements were adapted from those in the literature (Krishnamoorthy et al., 2011; Ramachandran & Viswanathamurthi, 2013). Data reproducibility was confirmed by conducting each experiment in triplicate and the standard equation shown below was used to determine the experimental percentage radical scavenging activities:

$$\%\ Radical\ scavenging\ activity = \left(\frac{A_c - A_f}{A_c}\right) x\ 100 \quad \text{(B)}$$

where the absorbance of the control is A_c (NO or DPPH radicals) and A_f is the absorbance upon addition of the individual metal complexes to the control. The metal complex concentrations that induce 50% radical scavenging activity (IC_{50} values) could be readily calculated from their distinctive experimental percentage radical scavenging activities. An experiment was initiated by collecting the UV-Vis spectrum of the control [DPPH (0.2 mM in MeOH)] followed by the addition of 0.1 mL of a metal complex (30 µM in DMSO) and then the sample solution was mixed to ensure homogeneity. Thereafter, the sample solution was incubated in the dark for 20 minutes and its UV-Vis spectrum was run.

(Atha et al., 2010)The following experimental technique was implemented for the NO radical assay: firstly, a 10 mM solution of sodium nitroprusside was prepared in PBS buffer and incubated for a 3-hour period at room temperature. Afterwards, Griess reagent (1 mL) was added to a 0.5 mL of the nitroprusside solution and the resultant solution constituted the control. Then the UV-Vis spectrum of the control was collected. A sample solution was prepared by the addition of a metal complex (30 µM in DMSO) to a 0.5 mL aliquot of sodium nitroprusside.

After a 3-hour incubation period, 1 mL of the Griess reagent was added to a sample solution and its UV-Vis spectrum was run.

2.4 BSA binding interaction studies

The BSA stock solution was prepared in PBS buffer at a pH of 7.2 and the concentration of this stock solution was determined spectrophotometrically using the extinction coefficient of 43824 M^{-1} cm^{-1} at 280 nm (Atha et al., 2010). Due to the considerable insolubility of **1** - **4** in the buffer, stock solutions (1.0 mM) of the metal complexes were prepared in acetonitrile. Data correction was implemented to the quenching titration studies to compensate for the inner filter effect using the following equation (Nehru et al., 2020):

$$F_{cor} = F_{obs}\, x\, 10^{(A_1 + A_2)/2} \qquad (C)$$

where, F_{cor} and F_{obs} are designated as the corrected and observed fluorescence intensities, respectively, whereas A_1 and A_2 are defined as the absorbance values of each ratio of BSA and a metal complex at peak maxima of the excitation and emission wavelengths, respectively.

2.5.1 Electronic spectrophotometric titrations

The BSA interaction experiments were conducted by maintaining the BSA concentration (~16 µM) whilst varying the concentrations of the respective metal complexes (0 – ~40 µM). An incubation time of 2 minutes was used for each sample mixture. Equal volumes of a metal complex were added to both the reference and sample cells. The data from the absorbance titrations were fitted to the following equation:

$$\left[\frac{A_o}{A_o - A}\right] = \left(\frac{\varepsilon_{BSA}}{\varepsilon_B}\right) + \left(\frac{\varepsilon_{BSA}}{\varepsilon_B . K_{app}}\right) . \left(\frac{1}{C_{metal\ complex}}\right) \qquad (D)$$

where A and A_0 are the absorbance values of BSA at 280 nm in the presence and absence of a metal complex, ε_{BSA} and ε_B are the extinction coefficients of BSA and the bound complex (*viz.* adduct of a metal complex and BSA), $C_{metal\ complex}$ is the concentration of a metal complex and K_{app} is the apparent association constant. From the equation (**D**), the following double reciprocal plot can be generated and the apparent association constant (K_{app}) is determined from the ratio of the intercept to the slope (Zhong et al., 2004).

$$\frac{1}{(A_o - A)} \; vs \left(\frac{1}{C_{metal\ complex}}\right)$$

2.5.2 Fluorescence emission spectroscopic titrations

The effects of increasing the metal complex concentrations on the emission spectrum of BSA were assessed. Fluorescence emission spectra were recorded at 293 K with the width of emission and excitation slits adjusted to 5 nm. The spectra were recorded in the wavelength range of 300 – 500 nm at an excitation wavelength of 280 nm. The resulting data was used to calculate the Stern-Volmer constant (K_{SV}) using the Stern-Volmer relationship (Paul et al., 2013):

$$\frac{F_0}{F} = 1 + K_{SV}\,[Q] \qquad \text{(E)}$$

where F_o and F are the emission intensities in the absence and presence of the metal complexes, respectively. The concentration of the respective metal complex is designated by [Q]. The K_{SV} values were obtained from the slope of the plot:

$$\frac{F_0}{F} \; vs \; [Q]$$

The quenching rate constant (k_q) can then be determined from equation (**F**):

$$K_{SV} = k_q \, \tau_0 \qquad \text{(F)}$$

where τ_0 is the lifetime of the protein (10^{-8} s) without a quencher.

The binding constants (K_b) and the binding number (n) can be quantified using equation (**G**) (Nehru et al., 2020):

$$Log \frac{(F_0 - F)}{F} = Log\, K_b + n\, Log\, [Q] \qquad \text{(G)}$$

where F_0, F and $[Q]$ are the same as in equation (**E**), K_b is the binding constant of each metal complex with BSA and *n* refers to the number of binding sites per BSA molecule, which can be determined from the following plot based on equation (**G**):

$$\frac{Log\,[F_o - F]}{F} \; vs \; Log\,[Q]$$

2.6 In vitro anticancer cell line studies

The cytotoxicity of the metal complexes against the HeLa and HCC70 triple negative breast carcinoma cell lines were determined using the MTT assay as previously described (de la Mare et al., 2012). In this assay, metabolically active cells convert the MTT dye to a blue formazan product that can be detected spectrophotometrically. Briefly, cells were seeded in a 96 well plate in complete medium, allowed to adhere overnight and incubated with a selective concentration range for the metal complexes (including a vehicle control and positive controls: 5-Fluorouracil and Paclitaxel in triplicate for 96-hours). Thereafter, the cells were incubated with MTT reagent for 4 hours, the resulting formazan crystals solubilized in SDS solution overnight and the absorbance at 595 nm measured. The IC_{50} values were calculated using non-linear regression in GraphPad Prism 4.0.

3. Results and discussion

3.1 Synthesis, spectral characterization and redox properties of 1 and 2

The diamagnetic metal complexes **1** and **2** were isolated in moderate yields by separate equimolar reactions of ombb and bbb with *trans*-$[RuCl_2(PPh_3)_3]$ in methanol. The source of the PF_6^- counter-ion of **1** emanates from the addition of ammonium hexafluorophosphate in an equivalent molar amount with respect to the metal precursor. For **1**, the *bis*-heterocyclic ligand (ombb) functions as a neutral tridentate chelator whereby coordination occurs through the benzimidazole nitrogen and bridging ether oxygen donor atoms. In the case of **2**, the ligand bbb coordinates *via* its neutral $N_{py}N_{py}$ donor set affording a constrained five-membered chelate ring *trans*-orientated to the *cis*-chloride co-ligands. These diamagnetic metal complexes were found to be stable in air as well as soluble in high boiling point aprotic solvents (*viz.* DMSO and DMF), while they exhibit moderate solubility in chlorinated solvents.

Generally, the signals of **1** and **2** in their ^{1}H NMR spectra display shifts with respect to analogous signals found in the proton spectra of their free ligands. These spectral differences resemble coordination of organic chelators to transition metal centers, see **Figs. S6** and **S7** (Haddad, Yousif, & Ahmed, 2013). In particular, the aromatic protons associated with the benzimidazole phenyl rings are shielded upon coordination of the ombb (in **1**) and bbb (in **2**)

organic chelators. Common to both proton spectra of the metal complexes is the presence of the intense multiplets within the region of 7.65 – 7.04 ppm, which are characteristic of the triphenylphosphine co-ligands (Satyanarayana & Reddy, 1987). Furthermore, the singlet associated with the methylene protons adjacent to the ethereal oxygen (*viz. H5, H5', H6 and H6'*) in **1** displays a noticeable shift from 5.39 to 5.31 ppm, which is attributed to ring current effects of the chelating aromatic benzimidazole, and these proton NMR spectral changes provide tangible evidence of O-coordination (Mikata, Fujimoto, Fujiwara, & Kondo, 2011; Stojcevic & Baird, 2009). A single peak was observed in each decoupled ^{31}P NMR spectra, which confirmed the presence of magnetically equivalent phosphorous atoms within the coordination spheres of the respective metal complexes, see **Figs. S8** and **S9**.

The solid-state infrared spectra of **1** and **2** illustrate their intense intracyclic ν(C=N) [1431 cm^{-1} for **1** and **2**] which are found at lower wavenumber in comparison to those found in the IR spectra of their free-ligands, ombb (at 1459 cm^{-1}) and bbb (at 1441 cm^{-1}), see **Figs. S10** and **S11**. The same trend is observed when comparing the coordinated (at 1088 cm^{-1}) and uncoordinated (at 1142 cm^{-1} for ombb) ether stretches of **1** and its corresponding free-ligand, which is also another influential feature of coordinative bonding. The dominating infrared experimental stretches (at 690 cm^{-1} for **1** and 692 cm^{-1} for **2**) in the respective IR spectra of the metal complexes are typical of ν(Ru-P) and are similar to those found in other metal complexes (Irvin N. Booysen, Adebisi, Akerman, Munro, & Xulu, 2016; Irvin Noel Booysen, Maikoo, Piers Akerman, Xulu, & Munro, 2013).

As expected, the electronic spectra of the metal complexes show several intense intraligand π-π* electronic transitions below 300 (for **1**) and 400 nm (for **2**), which mostly originate from the *pi*-conjugated moieties of their respective organic chelators, see **Figs. S12** and **S13**. At more red-shifted regions between 400 and 600 nm, p(Cl) → d(Ru) Ligand-to-Metal Charge Transfer (LMCT) bands are found. A distinctive metal-based electronic transition is found in the UV-Vis spectrum of **2** (at 712 nm) converse to the absence of a *d-d* electronic transition in the UV-Vis spectrum of **1,** which is largely ascribed to the low spin d^6 electron configuration of its central metal ion (Adebisi et al., 2016).

The redox properties of the metal complexes were investigated by means of voltammetric experiments. The cyclic voltammogram (CV) of **1** displays a one irreversible redox process (E_{pa}

= 1.36 V *vs* Ag | AgCl), which is attributed to the single electron oxidation of the metal center, while a quasi-reversible redox process [ΔE_p(**2**) = 80 mV and ΔE_p(ferrocene) = 90 mV] is found in the CV of **2** (E_{pa} = 0.42 V and E_{pc} = 0.34 V *vs* Ag| AgCl) attributed to the d^5/d^6 system interconversion, see **Figs. S14** and **S15**. Literature trends corroborate the assignment of the redox processes, *e.g.* the CVs of ruthenium(II) complex salts, [Ru(η^5-C_5H_5)(PPh_3)$_2$(L)](PF_6) (HL = 5-phenyl-1*H*-tetrazole and imidazole) display one irreversible oxidation process each at E_{pa} = 1.22 V and 1.25 V, respectively (Moreno et al., 2010).

3.2 Antioxidant studies

Oxidative stress has been implicated as one of the major causes of DNA mutation and excessive free radical concentrations in the blood stream can escalate cancer progression (Pizzino et al., 2017). Natural antioxidants such as Vitamin C are often not potent enough to inhibit the exponential growth of cancerous tumors induced by free radicals. Metal complexes have been shown to be highly effective scavengers of various free radicals, which largely stems from the redox active metal center and its organic ligand's capabilities to donate an electron and proton, respectively (Bal-Demirci et al., 2015; Sathiya Kamatchi, Chitrapriya, Kim, Fronczek, & Natarajan, 2013). The radical scavenging activities of the metal complexes **1** – **4** were investigated towards the NO and DPPH radicals, respectively, refer to **Table 1**.

The low IC_{50} values (**Table 1**) of the metal complexes strongly supports their exceptional antioxidant activities, which are shown to be more potent than the standard antioxidant vitamin C [IC_{50} (DPPH) = 141 µM; IC_{50} (NO) = 210 µM]. These favorable IC_{50} values could be ascribed to the attached ligands acting synergistically to enhance the radical scavenging activity of **1** – **4**, as benzimdazole and benzothiazole derivatives are known to possess good antioxidant properties (Ayhan-Kilcigil et al., 2005; Prouillac, Vicendo, Garrigues, Poteau, & Rima, 2009). The higher antioxidant activities for the paramagnetic metal complex **3** can be explained by the unpaired electron in the low spin d^5 orbital, which increases the propensity of the metal complex cation of **3** to neutralize the DPPH and NO free-radicals more effectively. The acidity of any available protons on the ligands may also be increased due to the electron deficient Ru(III) metal center, which may also positively impact the radical scavenging capability of the metal complex (Prakash, Manikandan, Viswanathamurthi, Velmurugan, & Nandhakumar, 2014). The obtained

IC_{50} values are within the range of those obtained for other documented metal complexes, for example, the IC_{50} values for some metal complexes were reported to be within the ranges of 24.0 – 59.7 µM and 6.7 – 11 µM for the DPPH and NO radicals respectively (Ramachandran & Viswanathamurthi, 2013).

3.3 DNA interaction studies

The potential of transition metal complexes as chemotherapeutic drugs can be readily gauged from their affinities to DNA (Galindo-Murillo, García-Ramos, Ruiz-Azuara, Cheatham, & Cortés-Guzmán, 2015). These metal complexes have illustrated diverse DNA interaction modes; for instance, their metal centers can directly coordinate to donor atoms within the DNA double helix or these metal complexes can facilely form DNA adducts *via* DNA intercalation between the DNA base pairs, resulting in major- or minor DNA groove binding (Pages et al., 2015). Numerous methods have been utilized to monitor the progressive formation of DNA-metal complex adducts, however one of the most versatile and simplest techniques is UV-Vis spectrophotometry (Hajian & Guan Huat, 2013).

Electronic spectral changes associated with DNA intercalation usually entails the decrementing absorbance of an aromatic chromophore's intra-ligand transition (*viz.* hypochromism) accompanied with a progressive red shift of the corresponding wavelength maximum (*viz.* bathochromism) (Bhattacharya & Mandal, 1997). These UV-Vis spectral alterations are accounted to *pi*-stacking interactions between a *pi*-conjugated chelator and the DNA base pairs (Shahabadi, Mohammadi, & Alizadeh, 2011). The contradictory UV-Vis spectral observations, the hyperchromic effect can arise from groove-binding as well as electrostatic attractions between the DNA and metal complex. Hypochromism is known to compromise the structural integrity of DNA by inducing denaturation or cleavage (Sirajuddin, Ali, & Badshah, 2013).

The UV-Vis spectral profiles depicting the DNA binding titrations for **1** and **2** reveal hypochromism (2.15 % at λ_{max} = 347 nm and 21.14 % at λ_{max} = 379 nm) with red shifts of 3 nm and 4 nm, respectively, see **Fig. 2**. In addition, diffuse isosbestic points are observed at 295, 361 and 511 nm in the UV-Vis spectral profile of **2,** which indicates that the metal complex exhibits a homogenous binding mode towards DNA. Synonymously, the arene metal complex, [(η^6-

$C_{12}H_{18}$)RuCl(PFPdpm)] [PFPdpm = 5-(penta-fluoro)phenyldipyrromethene] showed red shifts (of approximately 2 nm) for its intra-ligand and MLCT bands accompanied with gradual decreases in the absorbance values (under 10% hypochromism) during its CT-DNA binding electronic spectrophotometric experiment (Paitandi et al., 2017). The steric demands of the *cis*-$[Ru(PPh_3)_2]^{2+}$ core affords a significantly lower intrinsic binding constant for **1** (K_b =1.5 *x* 10^5 M^{-1}) (Motswainyana & Ajibade, 2015). Similarly, a carbonyl metal complex, $[RuCl(CO)(dppb)(bipy)]PF_6$ illustrated hypochromic behavior, however its sterically crowded bis(diphenylphosphine)butane (dppb) co-ligand impeded DNA intercalation and favored groove-binding based on its lower K_b (3.78 *x* 10^4 M^{-1}) value in comparison to ethidium bromide with a K_b value of 10^6 M^{-1} as well as other metal-based DNA intercalators (Carnizello et al., 2016) (Cory, McKee, Kagan, Henry, & Miller, 1985; Gao et al., 2008). Comparatively, the larger intrinsic binding constant (K_b) of **2** (1.2 *x* 10^7 M^{-1}) is higher than that obtained for [(η^6-$C_{12}H_{18}$)RuCl(PFPdpm)] (6.5 *x* 10^4 M^{-1}), which hints at multimodal interactions of **2** with CT-DNA. Thus, the metal complexes **1** and **2** can be regarded as preferential groove-binders.

Diverse spectral alterations were observed in the overlay electronic spectra of **4** upon its titration with CT-DNA, attesting to this metal complex's variable DNA interactive modes. Individual decreasing (λ_{max} = 294 nm) and increasing (λ_{max} = 329 nm) intraligand transitions are bridged by an isosbestic point appearing at 308 nm, while similarly, a broad shoulder centralized at 390 nm disappears with the appearance of a low intensity MLCT band at 517 nm. These UV-Vis spectral changes are symbolic of stereoelectronic redistributions with Hobz organic chelators of **3** upon interaction with CT-DNA. Of particular interest is the appearance of the metal-based electronic transition, which is suggestive of the metal center reducing and, hypothetically, this arises from coordinative bonding of the ruthenium to selected DNA base pairs. Analogous to the *bis*-heterocyclics (**1** and **2**), hypochromism (18 %) of **3**'s intra-ligand transition (monitored at 331 nm) is observed, which is accompanied by the disappearance of a very low-intensity *d-d* transition band at 639 nm. In addition, a clear appearance of a distinct MLCT band is detected at 416 nm, which again indicates reduction of the metal center upon coordination with the CT-DNA structure (as in the case of **3**). The calculated intrinsic binding constants (9 *x* 10^4 M^{-1} for **3** and 2 *x* 10^5 M^{-1} for **4**) of the mono-heterocyclic metal complexes are both smaller in magnitude than classical intercalators, which suggest that metal complexes **3** and **4** are predominately DNA groove-binders (Gao et al., 2008). Furthermore, the metal complexes **1** – **4** have similar intrinsic

binding constants (K_b) to the classical groove-binder, Hoechst-33342, and its analogues with K_b values ranging from 3×10^5 M^{-1} to 7×10^6 M^{-1} (Bazhulina et al., 2009; Loontiens, Regenfuss, Zechel, Dumortier, & Clegg, 1990; McGowan et al., 1988; Stokke & Steen, 1985).

The UV Agarose gel electrophoresis of human genomic DNA isolated from cancer cell lines demonstrated that each of the metal complexes could interact with DNA and resulted in a reduction in the fluorescence intensity of ethidium bromide (EtBr) staining. In particular, metal complexes **1** and **2** demonstrated a dose-dependent and significant reduction in fluorescence intensity of EtBr staining (**Fig. 3**). The extent of the metal complexes' DNA interactive capabilities can be directly correlated to the corresponding apparent DNA binding constants where **1** and **2** have higher intrinsic DNA binding constants and afford substantial reduction in the fluorescence intensity of EtBr. Furthermore, the Hoechst DNA binding competition studies corroborate that the metal complexes **1** – **4** are DNA groove-binders, see **Fig. S16**. In particular, the concentration-dependent studies affirm that the respective metal complexes exhibit gradually higher DNA binding affinities than the classical DNA groove-binder, Hoechst-33342.

3.4 BSA interaction studies

Serum albumins are major dissoluble proteins in the circulatory system and serve as primary transport media for numerous pharmaceuticals and physiologically relevant metal complexes (Milutinović et al., 2017). In particular, the affinity of a pharmaceutical to albumin has a significant influence on its pharmacokinetics. Mechanistically, the drug carrier protein can induce the careful reversible uptake and release of pharmaceuticals through altering its flexible structure while retaining its structural integrity. Primarily, medicinal inorganic complexes and organic compounds have been shown to bind to BSA domains IIA and IIIA subdomains (Karami, Alinaghi, Amirghofran, & Lipkowski, 2018).

Biomolecular titrations between the *in vivo* drug carrier protein, BSA and the respective metal complexes **1** - **4** were monitored using UV-Vis spectrophotometry and fluorescence emission spectroscopy. Gradual variations in intensities are indications of the conformational changes in the BSA structure induced by the additions of the individual metal complexes whilst any shifts in the electronic spectral bands reveals whether a metal complex is bound to the BSA

chromophore in its hydrophobic or hydrophilic environments (Paul et al., 2013; Zhong et al., 2004). Data attained from the electronic spectrophotometric titrations illustrated distinct hyperchromism accompanied by slight blue-shifts which are observed in the separate UV-Vis spectra of **1**, **2** and **3**, see **Fig. 4** and **S17**. These spectral observations concur with literature trends which suggests that minor unwinding of the protein strands occur leading to non-exposure of the polar tryptophan residues' microenvironment of BSA, for hydrogen-bonding interactions with water molecules (Cheng, Liu, & jiang, 2013).

Similarly, the distinguishing absorption band of BSA gradually increased upon interaction with **4,** however a minor red-shift of the peak maxima was noted. The aforementioned electronic spectral changes are attributed to the structural BSA integrity being compromised by its interaction with the metal complex. Consequently, the unfolding protein backbone exposes the tryptophan residues to aqueous media rendering increasing polarity and hydrophilicity for the BSA chromophore (Suryawanshi, Walekar, Gore, Anbhule, & Kolekar, 2016; Wu, Lin, Zhai, Zhuo, & Zhu, 2013). An explanation for the difference in trends could be explained by the larger number of hydrogen-bonding sites on metal complexes **1** – **3**, which results in more stable adduct formations with BSA. As a result, less unfolding of the protein backbone occurs which keeps the tryptophan residues unexposed and well-hidden in the hydrophobic protein cavity (Herskovits, Gadegbeku, & Jaillet, 1970; Mishra, Malakar, Biswal, Barman, & Krishnamoorthy, 2015).

From the double reciprocal plots of $1 / (A_0 - A)$ versus $1 / C_{metal\ complex}$, the apparent association constants (K_{app}) for **1**, **2**, **3** and **4** were calculated to be $1.80 \times 10^5\ M^{-1}$, $7.47 \times 10^6\ M^{-1}$, $4.66 \times 10^4\ M^{-1}$ and $2.00 \times 10^4\ M^{-1}$, respectively. These apparent association constants (K_{app}) are of similar magnitude to those obtained for other metal complexes and moreover, the K_{app} values can also denote ideal binding affinities towards BSA, which are considered to be between $10^4 - 10^6\ M^{-1}$ (Ravi Kumar et al., 2017; Topală, Bodoki, Oprean, & Oprean, 2014; Wong et al., 2014). The larger association constants linked with the *bis*-heterocyclic metal complexes **1** and **2** can be attributed to their larger sizes which allows more favourable hydrophobic interaction with the BSA interfacial surface. The presence of the chloride co-ligands also promotes higher reactivities as the halides are known to undergo *in vivo* ligand substitution to form aqua adducts that generate active coordination centres (Messori, Orioli, Vullo, Alessio, & Iengo, 2000).

BSA readily undergoes fluorescence quenching if one or more of its accessible domains are occupied by a quencher, which in the process leads to increasing concentrations of the non-fluorescent active BSA-quencher. Similarly to the UV-Vis spectrophotometry titration analysis, any changes in the conformation or environment of BSA due to interactions with a metal complex can result in quenching, with shifts in the characteristic BSA emission peak (Varlan & Hillebrand, 2010). Steady-state fluorescence quenching of BSA peak maximum occurs in the presence of all metal complexes, which affirms the formation of the BSA-metal complex aggregates, see **Figs. 5** and **S18**.

Blue-shifts in the BSA peak maxima occurs upon interaction with **1**, **2** and **3**, whereas a red-shift is observed when the protein is titrated against **4**. These findings are consistent with those found in the molecular absorption spectrophotometric titrations, whereby metal complexes **1** – **3** induces less unfolding of the protein thus keeping the BSA chromophore in a more hydrophobic environment, while metal complex **4** bares the BSA chromophore to an enhanced hydrophilic environment by increasing protein unfolding (Ojha & Das, 2011). The Stern-Volmer (K_{SV}) and quenching rate (k_q) constants were derived from the Stern-Volmer relationship and are shown in **Table 2**, see **Fig. 6**.

The obtained k_q values indicated that the fluorescence decay is a process of static quenching since these values are of a larger magnitude than that of quenchers involved in a dynamic equilibrium process (2×10^{10} M^{-1} s^{-1}) (Ramachandran & Viswanathamurthi, 2013; Varlan & Hillebrand, 2010). Since K_{SV} is the Stern-Volmer constant for static quenching, it can be used to examine the binding behaviour of the respective metal complexes towards BSA. The results conclude that the *bis*-heterocyclic metal complexes (**1** and **2**) exhibit higher binding affinities for BSA than the *mono*-heterocyclic metal complexes (**3** and **4**), which is consistent with the findings presented in the UV-Vis spectrophotometric analysis. Stern-Volmer (K_{SV}) and quenching rate (k_q) constants of similar magnitude were documented for other metal complexes, for example, *cis*-[Ru(quin)(dppm)$_2$]PF_6 [quin = quinaldate; dppm = *bis*(diphenylphosphino)methane] display K_{SV} and k_q values of 0.77×10^5 M^{-1} and 1.10×10^{13} M^{-1} s^{-1}, respectively (da Silva et al., 2017).

In the case of static quenching mechanisms, it can be presumed that there are comparable and independent binding sites within the BSA biomolecule. Therefore, the binding constant (K_b)

and the number of binding sites (*n*) could be determined using a modified version of the Stern-Volmer equation (**Equation G**). The calculated K_b suggests robust binding interactions for **1** (8.34×10^4 M^{-1}) and **4** (1.27×10^3 M^{-1}) with BSA, as metal complexes having binding constants ranging from 10^3 - 10^5 M^{-1} are considered strong binders (Kamtekar et al., 2013). Consequently, these results emphasize stable adduct formations for **1** and **4** when binding to BSA, respectively. Similar K_b values have been reported for the interaction of metal complexes with albumins in literature, for example, [(η^6-*p*-cymene)Ru(ATSC)Cl]PF_6 (ATSC = 9-anthraldehyde thiosemicarbazone) exhibited a K_b value of 12.1×10^4 (Beckford, 2010). In contrast, the lower K_b values for **2** (6.65×10^2 M^{-1}) and **3** (5.79×10^1 M^{-1}) were not expected as they were seen to be effective quenchers of BSA in the previous study, which implies weaker binding with BSA due to possible low plasma distribution (Nišavić et al., 2018). The *n* values obtained for all metal complexes are approaching unity, which indicate only one binding site for each metal complex occurred when binding to the BSA structure (Cheng et al., 2013).

3.5 In vitro anti-cancer activity

The cytotoxicity of the metal complexes **1** – **4** against the two cancer cell lines were assessed using an MTT assay and the results are shown in **Table 3**. The commonly used chemotherapeutics 5-FU and paclitaxel were included as positive controls and displayed cytotoxicity against HCC70 cells, with IC_{50} values of 127.07 (± 8.61) µM and 3.06 ± 1.11 nM, respectively. The metal complexes showed greater cytotoxicity than 5-FU but lower cytotoxicity than paclitaxel in HCC70 cells with IC_{50} values of 88.20 (± 1.10), 44.07 (± 1.12) and 39.37 (± 1.15) µM, for metal complexes **1**, **3** and **4**, respectively. The metal complexes were, however, more toxic than paclitaxel in HeLa cervical cancer cells (IC_{50} values of 17.42 ± 1.14, 16.59 ± 1.16 and 26.13 ± 1.16 µM, respectively). On the other hand, metal complex **2** was non-toxic to HCC70 and HeLa cells. The non-toxicity of **2** could be due to its lower cell membrane permeability despite it having comparable DNA interactive capabilities to the other metal complexes (Refat, Sharshar, Elsabawy, El-Sayed, & Adam, 2016). In addition, the metal complexes **1** - **4** exhibited significantly lower anti-cancer cellular activities than that of the antineoplastic drug, paclitaxel.

4. Conclusion

This research study demonstrated the DNA/ BSA interaction and antioxidant studies of diamagnetic and paramagnetic metal complexes bearing *mono*- or *bis*-heterocyclic chelates. The paramagnetic metal complex **3** showed the highest radical scavenging activities, which was ascribed to its d^5 metal center enhancing its propensity to neutralize NO and DPPH radicals. Steric factors of the metal complexes, such as their triphenylphosphine co-ligands, impeded DNA intercalation and led to the preferential DNA groove binding mode for these metal complexes. Groove binding interactions of the *bis*-heterocyclic metal complexes are dictated by electrostatic attractions whereas the DNA adducts of the metal complexes with the *mono*-heterocyclic chelates could also be stabilized by direct coordination to the DNA base pairs. Electronic and fluorescence BSA titration spectral data of **1** – **3** portrayed unwinding of the protein strands while that of **4** is characteristic of exposure of the tryptophan residues to aqueous media due the unfolding protein backbone. Steady-state quenching experiments show that the interaction of each metal complex with BSA adhere to a static mechanism with single binding sites. In addition, the *mono*-heterocyclic metal complexes showed weaker binding affinities than the *bis*-heterocyclic metal complexes based on the trends in the calculated K_{SV} and K_{app} values. Low cytotoxicity of the metal complex **2** which was accounted to poor cell permeability, while the other metal complexes showed superior *in vitro* anticancer activities than 5-FU.

Supporting Information Document

CCDC 1866502 contains the supplementary crystallographic data for this paper. These data can be obtained free of charge from The Cambridge Crystallographic Data Centre *via* www.ccdc.cam.ac.uk/data_request/cif. Supplementary figures **S1**-**S26** associated with this article can be found in the online version.

Acknowledgements:

This research was supported by funding from the South African Research Chairs Initiative of the Department of Science and Technology (DST) and National Research Foundation of South Africa (NRF) (Grant No. 98566), NRF CPRR (Grant No. 105829), Thuthuka NRF (Research Grant No. 94020), Incentive Funding for Rated Researchers NRF (Research Grant No. 114737), Rhodes University and University of KwaZulu-Natal. The views expressed are those of the authors and should not be attributed to the DST, NRF, Rhodes University or University of KwaZulu-Natal. The authors would like to express their gratitude to Eric Hosten from Nelson Mandela University for attaining the low resolution structure of **1** and Matthew Akerman from the University of KwaZulu-Natal for attempting to fully refine it.

Declaration of interest statement:

The authors declare no conflict of interest.

References

Adebisi, A., Booysen, I. N., Akerman, M. P., & Xulu, B. (2016). Ruthenium complexes with lumazine derivatives: structural, electrochemical, computational and radical scavenging studies. *Transition Metal Chemistry, 41*(6), 629-635. doi:https://doi.org/10.1007/s11243-016-0062-3

Atha, D. H., Manne, U., Grizzle, W. E., Wagner, P. D., Srivastava, S., & Reipa, V. (2010). Standards for immunohistochemical imaging: a protein reference device for biomarker quantitation. *The journal of histochemistry and cytochemistry : official journal of the Histochemistry Society, 58*(11), 1005-1014. doi:https://doi.org/10.1369/jhc.2010.956342

Ayhan-Kilcigil, G., Kuş, C., Coban, T., Can-Eke, B., Ozbey, S., & Iscan, M. (2005). Synthesis, antioxidant and radical scavenging activities of novel benzimidazoles. *Journal of enzyme inhibition and medicinal chemistry, 20*(5), 503-514. doi:https://doi.org/10.1080/14756360500287086

Bal-Demirci, T., Şahin, M., Kondakçı, E., Özyürek, M., Ülküseven, B., & Apak, R. (2015). Synthesis and antioxidant activities of transition metal complexes based 3-hydroxysalicylaldehyde-S-methylthiosemicarbazone. *Spectrochimica Acta Part A:*

Molecular and Biomolecular Spectroscopy, *138*, 866-872. doi:https://doi.org/10.1016/j.saa.2014.10.088

Bazhulina, N. P., Nikitin, A. M., Rodin, S. A., Surovaya, A. N., Kravatsky, Y. V., Pismensky, V. F., . . . Gursky, G. V. (2009). Binding of Hoechst 33258 and its Derivatives to DNA. *Journal of Biomolecular Structure and Dynamics*, *26*(6), 701-718. doi:10.1080/07391102.2009.10507283

Beckford, F. A. (2010). Reaction of the Anticancer Organometallic Ruthenium Compound, [n6(p-Cymene)Ru(ATSC)Cl] with Human Serum Albumin. *International Journal of Inorganic Chemistry, 2010*, 975756. doi:10.1155/2010/975756

Bhattacharya, S., & Mandal, S. S. (1997). Interaction of surfactants with DNA. Role of hydrophobicity and surface charge on intercalation and DNA melting. *Biochimica et Biophysica Acta (BBA) - Biomembranes*, *1323*(1), 29-44. doi:https://doi.org/10.1016/S0005-2736(96)00171-X

Booysen, I. N., Adebisi, A., Akerman, M. P., Munro, O. Q., & Xulu, B. (2016). Coordination of di- and triimine ligands at ruthenium(II) and ruthenium(III) centers: structural, electrochemical and radical scavenging studies. *Journal of Coordination Chemistry*, *69*(10), 1641-1652. doi:10.1080/00958972.2016.1177177

Booysen, I. N., Maikoo, S., Piers Akerman, M., Xulu, B., & Munro, O. (2013). Ruthenium(II/IV) complexes with potentially tridentate Schiff base chelates containing the uracil moiety. *Journal of Coordination Chemistry*, *66*(20), 3673-3685. doi:10.1080/00958972.2013.849808

Carnizello, A. P., Barbosa, M. I. F., Martins, M., Ferreira, N. H., Oliveira, P. F., Magalhães, G. M., . . . Tavares, D. C. (2016). In vitro and in vivo antitumor activity of a novel carbonyl ruthenium compound, the ct-[RuCl(CO)(dppb)(bipy)]PF-6[dppb=1,4-bis(diphenylphosphine)butane and bipy=2,2′-bipyridine]. *Journal of Inorganic Biochemistry, 164*, 42-48. doi:https://doi.org/10.1016/j.jinorgbio.2016.08.010

Caruso, F., Pettinari, R., Rossi, M., Monti, E., Gariboldi, M. B., Marchetti, F., . . . Subbaraju, G. V. (2016). The in vitro antitumor activity of arene-ruthenium(II) curcuminoid complexes improves when decreasing curcumin polarity. *Journal of Inorganic Biochemistry, 162*, 44-51. doi:https://doi.org/10.1016/j.jinorgbio.2016.06.002

Chatterjee, S., Biondi, I., Dyson, P. J., & Bhattacharyya, A. (2011). A bifunctional organometallic ruthenium drug with multiple modes of inducing apoptosis. *JBIC Journal of Biological Inorganic Chemistry, 16*(5), 715-724. doi:10.1007/s00775-011-0772-0

Cheng, Z., Liu, R., & jiang, X. (2013). Spectroscopic studies on the interaction between tetrandrine and two serum albumins by chemometrics methods. *Spectrochimica Acta Part A: Molecular and Biomolecular Spectroscopy, 115*, 92-105. doi:https://doi.org/10.1016/j.saa.2013.06.007

Cory, M., McKee, D. D., Kagan, J., Henry, D. W., & Miller, J. A. (1985). Design, synthesis, and DNA binding properties of bifunctional intercalators. Comparison of polymethylene and diphenyl ether chains connecting phenanthridine. *Journal of the American Chemical Society, 107*(8), 2528-2536. doi:10.1021/ja00294a054

da Silva, E. N., da Silva, P. A. B., Graminha, A. E., de Oliveira, P. F., Damasceno, J. L., Tavares, D. C., . . . Von Poelhsitz, G. (2017). Synthesis, Characterization, Cytotoxic Activity, and Interactions with CT-DNA and BSA of Cationic Ruthenium(II) Complexes Containing Dppm and Quinoline Carboxylates. *Bioinorganic Chemistry and Applications, 2017*, 2562780. doi:https://doi.org/10.1155/2017/2562780

de la Mare, J.-A., Lawson, J. C., Chiwakata, M. T., Beukes, D. R., Edkins, A. L., & Blatch, G. L. (2012). Quinones and halogenated monoterpenes of algal origin show anti-proliferative effects against breast cancer cells in vitro. *Investigational new drugs, 30*(6), 2187-2200. doi:https://doi.org/10.1007/s10637-011-9788-0

Dwyer, B. G., Johnson, E., Cazares, E., McFarlane Holman, K. L., & Kirk, S. R. (2018). Ruthenium anticancer agent KP1019 binds more tightly than NAMI-A to tRNAPhe. *Journal of Inorganic Biochemistry, 182*, 177-183. doi:https://doi.org/10.1016/j.jinorgbio.2018.02.019

Galindo-Murillo, R., García-Ramos, J. C., Ruiz-Azuara, L., Cheatham, T. E., 3rd, & Cortés-Guzmán, F. (2015). Intercalation processes of copper complexes in DNA. *Nucleic acids research, 43*(11), 5364-5376. doi:https://doi.org/10.1093/nar/gkv467

Gao, F., Chao, H., Zhou, F., Chen, X., Wei, Y.-F., & Ji, L.-N. (2008). Synthesis, GC selective DNA binding and topoisomerase II inhibition activities of ruthenium(II) polypyridyl complex containing 11-aminopteridino[6,7-f][1,10]phenanthrolin-13(12H)-one. *Journal*

of Inorganic Biochemistry, 102(5), 1050-1059. doi:https://doi.org/10.1016/j.jinorgbio.2007.12.025

Haddad, R., Yousif, E., & Ahmed, A. (2013). Synthesis and characterization of transition metal complexes of 4-Amino-5-pyridyl-4H-1,2,4-triazole-3-thiol. *Springerplus, 2*, 510. doi:https://doi.org/10.1186/2193-1801-2-510

Hajian, R., & Guan Huat, T. (2013). Spectrophotometric Studies on the Thermodynamics of the ds-DNA Interaction with Irinotecan for a Better Understanding of Anticancer Drug-DNA Interactions. *Journal of Spectroscopy, 2013*, 380352. doi:https://doi.org/10.1155/2013/380352

Herskovits, T. T., Gadegbeku, B., & Jaillet, H. (1970). On the structural stability and solvent denaturation of proteins. I. Denaturation by the alcohols and glycols. *J Biol Chem, 245*(10), 2588-2598. doi:https://www.jbc.org/content/245/10/2588.long

Kamtekar, N., Pandey, A., Agrawal, N., Pissurlenkar, R. R., Borana, M., & Ahmad, B. (2013). Interaction of multimicrobial synthetic inhibitor 1,2-bis(2-benzimidazolyl)-1,2-ethanediol with serum albumin: spectroscopic and computational studies. *PLoS One, 8*(1), e53499. doi:https://doi.org/10.1371/journal.pone.0053499

Kaplanis, M., Stamatakis, G., Papakonstantinou, V. D., Paravatou-Petsotas, M., Demopoulos, C. A., & Mitsopoulou, C. A. (2014). Re(I) tricarbonyl complex of 1,10-phenanthroline-5,6-dione: DNA binding, cytotoxicity, anti-inflammatory and anti-coagulant effects towards platelet activating factor. *Journal of Inorganic Biochemistry, 135*, 1-9. doi:https://doi.org/10.1016/j.jinorgbio.2014.02.003

Karami, K., Alinaghi, M., Amirghofran, Z., & Lipkowski, J. (2018). Synthesis and characterization of two new trans palladium (II) complexes containing benzylamine ligand: DNA/BSA interactions, molecular docking and in vitro cytotoxic activity. *Inorganica Chimica Acta, 471*, 797-807. doi:https://doi.org/10.1016/j.ica.2017.02.027

Kopel, P., Wawrzak, D., Langer, V., Cihalova, K., Chudobova, D., Vesely, R., . . . Kizek, R. (2015). Biological Activity and Molecular Structures of Bis(benzimidazole) and Trithiocyanurate Complexes. *Molecules, 20*(6), 10360-10376. doi:https://doi.org/10.3390/molecules200610360

Krishnamoorthy, P., Sathyadevi, P., Senthilkumar, K., Muthiah, P. T., Ramesh, R., & Dharmaraj, N. (2011). Copper(I) hydrazone complexes: Synthesis, structure, DNA binding, radical

scavenging and computational studies. *Inorganic Chemistry Communications, 14*(9), 1318-1322. doi:https://doi.org/10.1016/j.inoche.2011.05.004

Lazarević, T., Rilak, A., & Bugarčić Ž, D. (2017). Platinum, palladium, gold and ruthenium complexes as anticancer agents: Current clinical uses, cytotoxicity studies and future perspectives. *Eur J Med Chem, 142*, 8-31. doi:https://doi.org/10.1016/j.ejmech.2017.04.007

Levina, A., Mitra, A., & Lay, P. A. (2009). Recent developments in ruthenium anticancer drugs. *Metallomics, 1*(6), 458-470. doi:https://doi.org/10.1039/B904071D

Loontiens, F. G., Regenfuss, P., Zechel, A., Dumortier, L., & Clegg, R. M. (1990). Binding characteristics of Hoechst 33258 with calf thymus DNA, poly[d(A-T)] and d(CCGGAATTCCGG): multiple stoichiometries and determination of tight binding with a wide spectrum of site affinities. *Biochemistry, 29*(38), 9029-9039. doi:https://doi.org/10.1021/bi00490a021

McGowan, P. F., Hurst, R. E., Bass, R. A., Wilcox, L. J., Hemstreet, G. P., & Postier, R. G. (1988). Equilibrium binding of Hoechst 33258 and Hoechst 33342 fluorochromes with rat colorectal cells. *Journal of Histochemistry & Cytochemistry, 36*(7), 757-762. doi:https://doi.org/10.1177/36.7.2454985

Merlino, A. (2016). Interactions between proteins and Ru compounds of medicinal interest: A structural perspective. *Coordination Chemistry Reviews, 326*, 111-134. doi:https://doi.org/10.1016/j.ccr.2016.08.001

Messori, L., Orioli, P., Vullo, D., Alessio, E., & Iengo, E. (2000). A spectroscopic study of the reaction of NAMI, a novel ruthenium(III)anti-neoplastic complex, with bovine serum albumin. *European Journal of Biochemistry, 267*(4), 1206-1213. doi:https://doi.org/10.1046/j.1432-1327.2000.01121.x

Mikata, Y., Fujimoto, T., Fujiwara, T., & Kondo, S.-i. (2011). Intramolecular ether oxygen coordination in the zinc complexes with dipicolylamine (DPA)-derived ligands. *Inorganica Chimica Acta, 370*(1), 420-426. doi:https://doi.org/10.1016/j.ica.2011.02.022

Milutinović, M. M., Rilak, A., Bratsos, I., Klisurić, O., Vraneš, M., Gligorijević, N., . . . Bugarčić, Ž. D. (2017). New 4′-(4-chlorophenyl)-2,2′:6′,2″-terpyridine ruthenium(II) complexes: Synthesis, characterization, interaction with DNA/BSA and cytotoxicity

studies. *Journal of Inorganic Biochemistry, 169*, 1-12. doi:https://doi.org/10.1016/j.jinorgbio.2016.10.001

Mishra, A., Malakar, A., Biswal, H. T., Barman, M. K., & Krishnamoorthy, G. (2015). Interactions of a few azole derivatives with a transport protein: role of heteroatoms. *Journal of Molecular Recognition, 28*(5), 299-305. doi:https://doi.org/10.1002/jmr.2444

Moreno, V., Lorenzo, J., Aviles, F. X., Garcia, M. H., Ribeiro, J. P., Morais, T. S., . . . Robalo, M. P. (2010). Studies of the Antiproliferative Activity of Ruthenium (II) Cyclopentadienyl-Derived Complexes with Nitrogen Coordinated Ligands. *Bioinorganic Chemistry and Applications, 2010*, 936834. doi:https://doi.org/10.1155/2010/936834

Motswainyana, W. M., & Ajibade, P. A. (2015). Anticancer Activities of Mononuclear Ruthenium(II) Coordination Complexes. *Advances in Chemistry, 2015*, 859730. doi:https://doi.org/10.1155/2015/859730

Nehru, S., Veeralakshmi, S., Kalaiselvam, S., Subin David, S. P., Sandhya, J., & Arunachalam, S. (2020). Protein binding and antioxidant studies of diimine based emissive surfactant–ruthenium(II) complexes. *Journal of Biomolecular Structure and Dynamics*, 1-12. doi:https://doi.org/10.1080/07391102.2020.1733664

Ng, N. S., Wu, M. J., & Aldrich-Wright, J. R. (2018). The cytotoxicity of some phenanthroline-based antimicrobial copper(II) and ruthenium(II) complexes. *Journal of Inorganic Biochemistry, 180*, 61-68. doi:https://doi.org/10.1016/j.jinorgbio.2017.11.022

Nišavić, M., Stoiljković, M., Crnolatac, I., Milošević, M., Rilak, A., & Masnikosa, R. (2018). Highly water-soluble ruthenium(II) terpyridine coordination compounds form stable adducts with blood-borne metal transporting proteins. *Arabian Journal of Chemistry, 11*(3), 291-304. doi:https://doi.org/10.1016/j.arabjc.2016.07.021

Ojha, B., & Das, G. (2011). Role of hydrophobic and polar interactions for BSA–amphiphile composites. *Chemistry and Physics of Lipids, 164*(2), 144-150. doi:https://doi.org/10.1016/j.chemphyslip.2010.12.004

Pages, B. J., Ang, D. L., Wright, E. P., & Aldrich-Wright, J. R. (2015). Metal complex interactions with DNA. *Dalton Transactions, 44*(8), 3505-3526. doi:https://doi.org/10.1039/C4DT02700K

Paitandi, R. P., Singh, R. S., Mukhopadhyay, S., Sharma, G., Koch, B., Vishnoi, P., & Pandey, D. S. (2017). Synthesis, characterization, DNA binding and cytotoxicity of fluoro-

dipyrrin based arene ruthenium(II) complexes. *Inorganica Chimica Acta*, *454*, 117-127. doi:https://doi.org/10.1016/j.ica.2016.03.003

Pastuszko, A., Majchrzak, K., Czyz, M., Kupcewicz, B., & Budzisz, E. (2016). The synthesis, lipophilicity and cytotoxic effects of new ruthenium(II) arene complexes with chromone derivatives. *Journal of Inorganic Biochemistry, 159*, 133-141. doi:https://doi.org/10.1016/j.jinorgbio.2016.02.020

Paul, H., Mukherjee, T., Mukherjee, M., Mondal, T. K., Moirangthem, A., Basu, A., . . . Chattopadhyay, P. (2013). Ruthenium(II) complexes of pyrrol-azo ligands: cytotoxicity, interaction with calf thymus DNA and bovine serum albumin. *Journal of Coordination Chemistry, 66*(15), 2747-2764. doi:https://doi.org/10.1080/00958972.2013.814048

Pizzino, G., Irrera, N., Cucinotta, M., Pallio, G., Mannino, F., Arcoraci, V., . . . Bitto, A. (2017). Oxidative Stress: Harms and Benefits for Human Health. *Oxidative Medicine and Cellular Longevity, 2017*, 8416763. doi:https://doi.org/10.1155/2017/8416763

Prakash, G., Manikandan, R., Viswanathamurthi, P., Velmurugan, K., & Nandhakumar, R. (2014). Ruthenium(III) S-methylisothiosemicarbazone Schiff base complexes bearing PPh3/AsPh3 coligand: Synthesis, structure and biological investigations, including antioxidant, DNA and protein interaction, and in vitro anticancer activities. *Journal of Photochemistry and Photobiology B: Biology, 138*, 63-74. doi:https://doi.org/10.1016/j.jphotobiol.2014.04.019

Prouillac, C., Vicendo, P., Garrigues, J.-C., Poteau, R., & Rima, G. (2009). Evaluation of new thiadiazoles and benzothiazoles as potential radioprotectors: free radical scavenging activity in vitro and theoretical studies (QSAR, DFT). *Free radical biology & medicine, 46*(8), 1139-1148. doi:https://doi.org/10.1016/j.freeradbiomed.2009.01.016

Ramachandran, R., & Viswanathamurthi, P. (2013). Ruthenium(II) carbonyl complexes containing pyridine carboxamide ligands and PPh3/AsPh3/Py coligands: Synthesis, spectral characterization, catalytic and antioxidant studies. *Spectrochimica Acta Part A: Molecular and Biomolecular Spectroscopy, 103*, 53-61. doi:https://doi.org/10.1016/j.saa.2012.10.072

Ravi Kumar, V., Nagababu, P., Srinivas, G., Rajender Reddy, M., Vinoda Rani, M., Ravi, M., & Satyanarayana, S. (2017). Investigation of DNA/BSA binding of three Ru(II) complexes by various spectroscopic methods, molecular docking and their antimicrobial activity.

Journal of Coordination Chemistry, *70*(22), 3790-3809. doi:https://doi.org/10.1080/00958972.2017.1407410

Refat, M. S., Sharshar, T., Elsabawy, K. M., El-Sayed, M. Y., & Adam, A. M. A. (2016). Synthesis, physicochemical characterization and anticancer screening of sulfa drug ruthenium complexes as anticancer agent. *Journal of Molecular Liquids, 222*, 334-349. doi:https://doi.org/10.1016/j.molliq.2016.07.006

Reichmann, M. E., Rice, S. A., Thomas, C. A., & Doty, P. (1954). A Further Examination of the Molecular Weight and Size of Desoxypentose Nucleic Acid. *Journal of the American Chemical Society, 76*(11), 3047-3053. doi:https://doi.org/10.1021/ja01640a067

Sathiya Kamatchi, T., Chitrapriya, N., Kim, S. K., Fronczek, F. R., & Natarajan, K. (2013). Influence of carboxylic acid functionalities in ruthenium (II) polypyridyl complexes on DNA binding, cytotoxicity and antioxidant activity: Synthesis, structure and in vitro anticancer activity. *European Journal of Medicinal Chemistry, 59*, 253-264. doi:https://doi.org/10.1016/j.ejmech.2012.11.024

Satyanarayana, T., & Reddy, K. V. (1987). Some benzimidazole amide complexes of ruthenium(II). *Proceedings of the Indian Academy of Sciences - Chemical Sciences, 99*(4), 237-242. doi:https://doi.org/10.1007/BF02881245

Shahabadi, N., Mohammadi, S., & Alizadeh, R. (2011). DNA Interaction Studies of a New Platinum(II) Complex Containing Different Aromatic Dinitrogen Ligands. *Bioinorganic Chemistry and Applications, 2011*, 429241. doi:https://doi.org/10.1155/2011/429241

Sirajuddin, M., Ali, S., & Badshah, A. (2013). Drug–DNA interactions and their study by UV–Visible, fluorescence spectroscopies and cyclic voltametry. *Journal of Photochemistry and Photobiology B: Biology*, *124*, 1-19. doi:https://doi.org/10.1016/j.jphotobiol.2013.03.013

Stojcevic, G., & Baird, M. C. (2009). An investigation of the influence of R on the abilities of the polar monomers CH2・CH(CH2)8OR (R = Me, PhCH2, Ph3C, Me3Si, Ph3Si) to participate in O- rather than η2-coordination to metallocene alkene polymerization catalysts; an unanticipated role for ether oxygen coordination in promoting polymerization. *Dalton Transactions*(41), 8864-8877. doi:https://doi.org/10.1039/B908726E

Stokke, T., & Steen, H. B. (1985). Multiple binding modes for Hoechst 33258 to DNA. *Journal of Histochemistry & Cytochemistry*, *33*(4), 333-338. doi:https://doi.org/10.1177/33.4.2579998

Suryawanshi, V. D., Walekar, L. S., Gore, A. H., Anbhule, P. V., & Kolekar, G. B. (2016). Spectroscopic analysis on the binding interaction of biologically active pyrimidine derivative with bovine serum albumin. *Journal of Pharmaceutical Analysis, 6*(1), 56-63. doi:https://doi.org/10.1016/j.jpha.2015.07.001

Swarnalatha, K., Rathnamala, P., Babu, A. A., & Bhuvanesh, N. (2016). Structural characterization, photophysical and BSA binding interaction studies of 4,4′-bis(benzimidazolyl)-2,2′-bipyridine. *Journal of Structural Chemistry*, 57(8), 1554-1560. doi:https://doi.org/10.1134/S0022476616080096

Taha, M., Ismail, N. H., Imran, S., Selvaraj, M., Rashwan, H., Farhanah, F. U., . . . Ali, M. (2015). Synthesis of benzimidazole derivatives as potent β-glucuronidase inhibitors. *Bioorganic Chemistry, 61*, 36-44. doi:https://doi.org/10.1016/j.bioorg.2015.05.010

Tavman, A., & Çinarli, A. (2014). Synthesis and spectral characterization of 1,3-bis-(1H-benzimidazol-2-yl)-2-oxapropane complexes with various Zn(II) salts. *Inorganica Chimica Acta, 421*, 481-488. doi:https://doi.org/10.1016/j.ica.2014.07.036

Thota, S., Rodrigues, D. A., Crans, D. C., & Barreiro, E. J. (2018). Ru(II) Compounds: Next-Generation Anticancer Metallotherapeutics? *Journal of Medicinal Chemistry*, *61*(14), 5805-5821. doi:10.1021/acs.jmedchem.7b01689

Topală, T., Bodoki, A., Oprean, L., & Oprean, R. (2014). Bovine Serum Albumin Interactions with Metal Complexes. *Clujul medical (1957), 87*(4), 215-219. doi:https://doi.org/10.15386/cjmed-357

Varlan, A., & Hillebrand, M. (2010). Bovine and human serum albumin interactions with 3-carboxyphenoxathiin studied by fluorescence and circular dichroism spectroscopy. *Molecules (Basel, Switzerland), 15*(6), 3905-3919. doi:https://doi.org/10.3390/molecules15063905

Wong, C.-Y., Chung, L.-H., Lin, S., Chan, D. S.-H., Leung, C.-H., & Ma, D.-L. (2014). A ruthenium(II) complex supported by trithiacyclononane and aromatic diimine ligand as luminescent switch-on probe for biomolecule detection and protein staining. *Scientific reports, 4*, 7136-7136. doi:https://doi.org/10.1038/srep07136

Wu, A.-Z., Lin, C.-Z., Zhai, Y.-J., Zhuo, J.-L., & Zhu, C.-C. (2013). Investigation of the interaction between two phenylethanoid glycosides and bovine serum albumin by spectroscopic methods. *Journal of Pharmaceutical Analysis, 3*(1), 61-65. doi:https://doi.org/10.1016/j.jpha.2012.07.001

Yadav, G., & Ganguly, S. (2015). Structure activity relationship (SAR) study of benzimidazole scaffold for different biological activities: A mini-review. *European Journal of Medicinal Chemistry, 97*, 419-443. doi:https://doi.org/10.1016/j.ejmech.2014.11.053

Yamin, G., & Teplow, D. B. (2017). Pittsburgh Compound-B (PiB) binds amyloid β-protein protofibrils. *Journal of Neurochemistry, 140*(2), 210-215. doi:https://doi.org/10.1111/jnc.13887

Zeng, L., Gupta, P., Chen, Y., Wang, E., Ji, L., Chao, H., & Chen, Z.-S. (2017). The development of anticancer ruthenium(ii) complexes: from single molecule compounds to nanomaterials. *Chemical Society Reviews, 46*(19), 5771-5804. doi:https://doi.org/10.1039/C7CS00195A

Zhang, P., & Sadler, P. J. (2017). Advances in the design of organometallic anticancer complexes. *Journal of Organometallic Chemistry, 839*, 5-14. doi:https://doi.org/10.1016/j.jorganchem.2017.03.038

Zhong, W., Wang, Y., Yu, J.-S., Liang, Y., Ni, K., & Tu, S. (2004). The interaction of human serum albumin with a novel antidiabetic agent—SU-118. *Journal of Pharmaceutical Sciences, 93*(4), 1039-1046. doi:10.1002/jps.20005

Figure 1: Structures of the respective metal complexes.

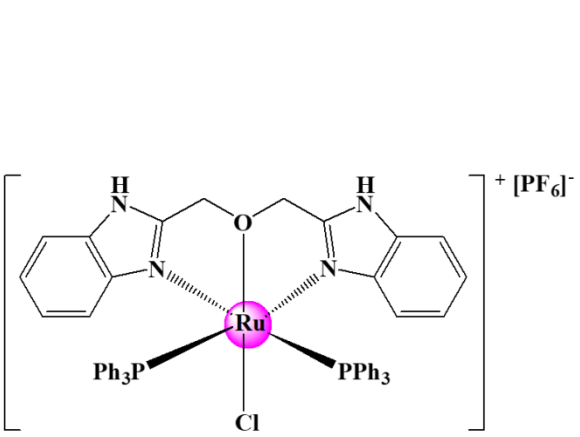

Metal complex 1

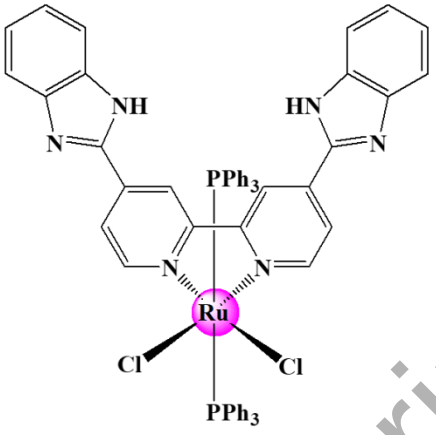

Metal complex 2

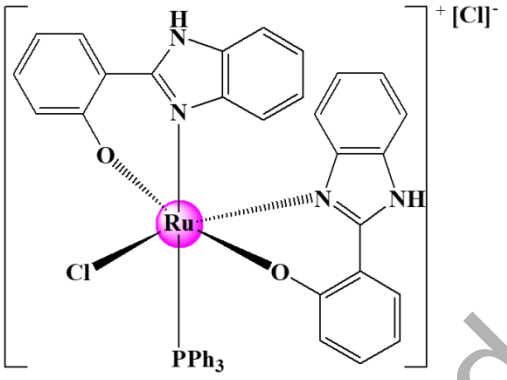

Metal complex 3

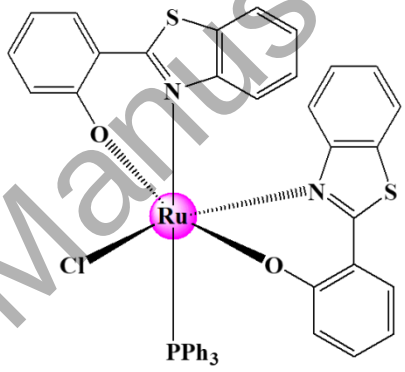

Metal complex 4

Figure 2: Overlay UV-Vis spectra of metal complexes **1** (a), **2** (b), **3** (c) and **4** (d) in the absence and presence of increasing amounts of CT-DNA. A dashed line indicates the initial spectrum. Volumes of DNA solutions ranges from 0 to 36 µL.

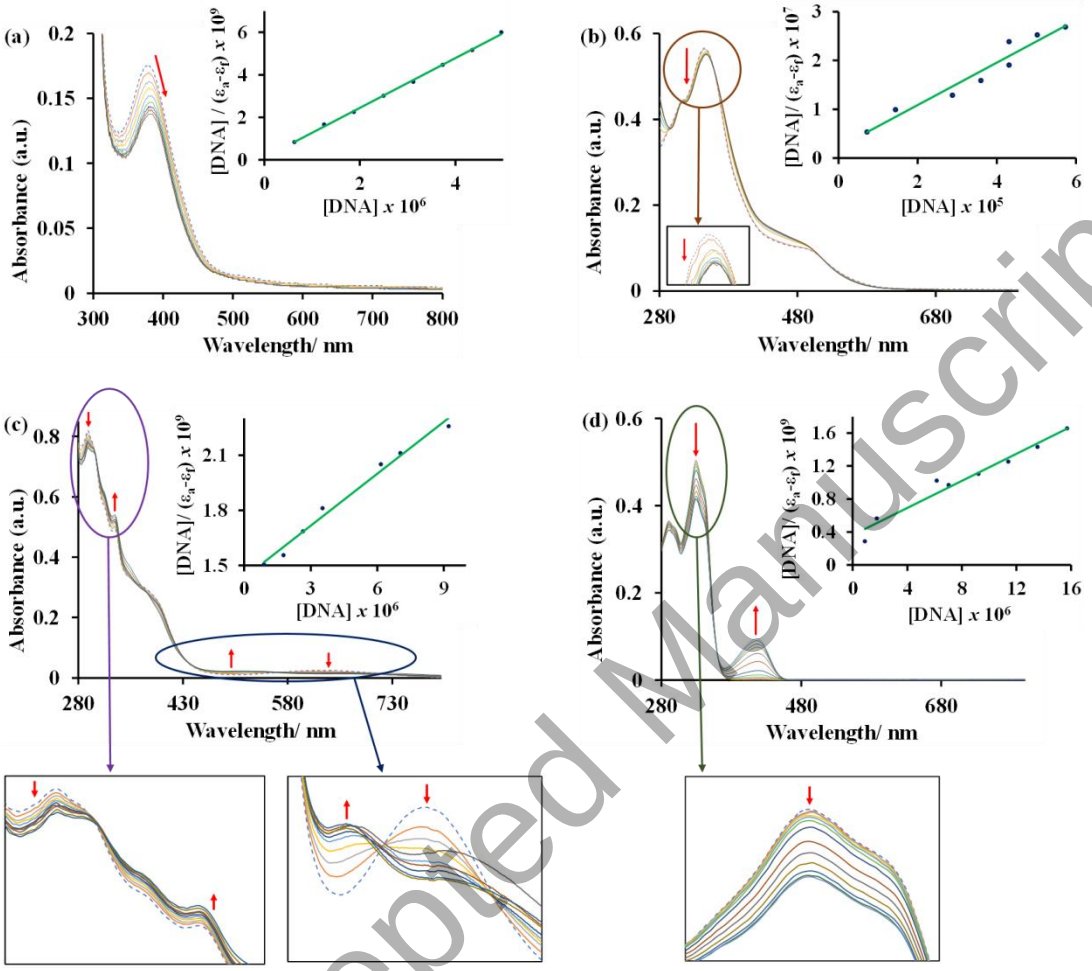

Fig. 3: Analysis of interaction of the metal complexes with human genomic DNA by agarose gel electrophoresis. The average fluorescence intensity of the DNA bands was quantified by ImageJ and is shown relative to the intensity of the DMSO control (± SEM, n=3). Statistical significance was assessed by two-way ANOVA with Bonferroni post-tests, where * indicates $p < 0.05$

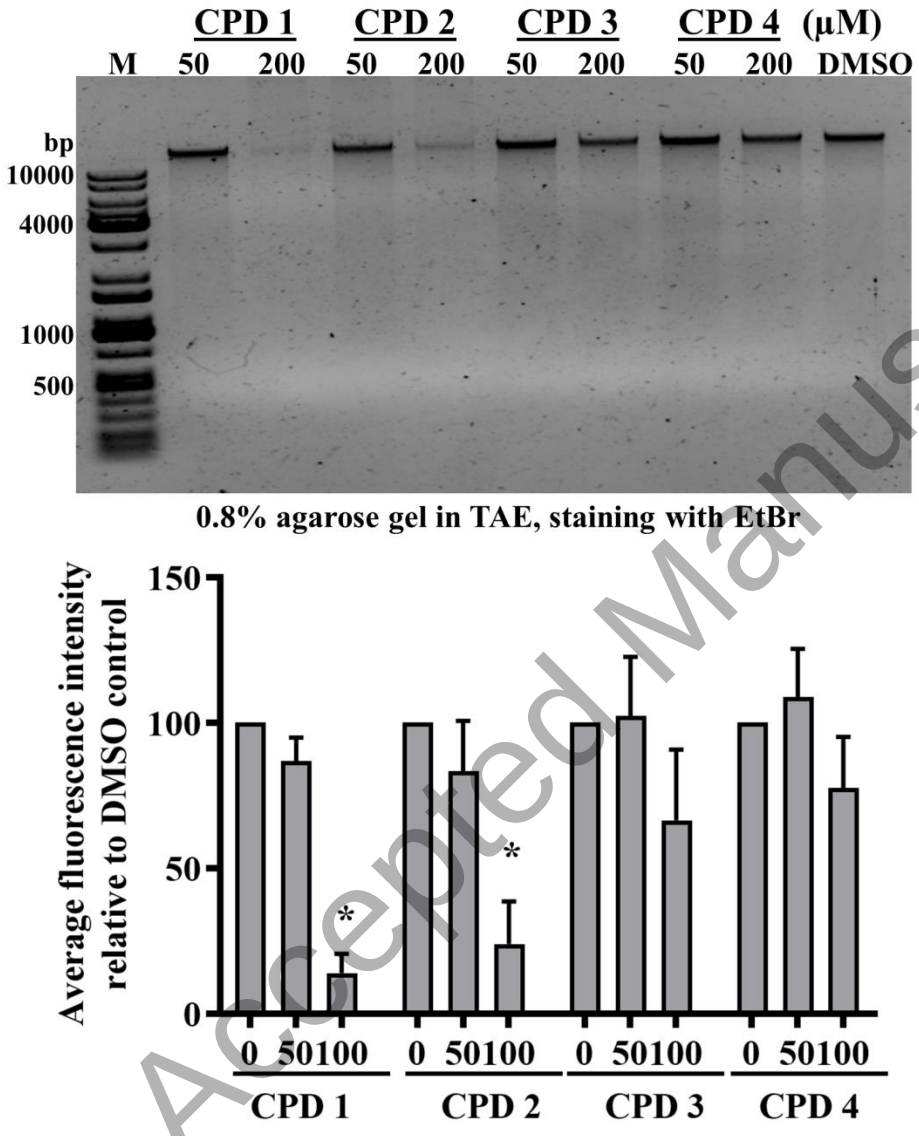

Fig. 4: UV-Vis spectral profile depicting the titration between metal complex **1** and BSA. The inset is the corresponding double reciprocal plot of $1 / (A_0 - A)$ versus $1 / C_{metal\ complex}$. Volumes of the standardized metal complex solutions range from 0 to 59 µL.

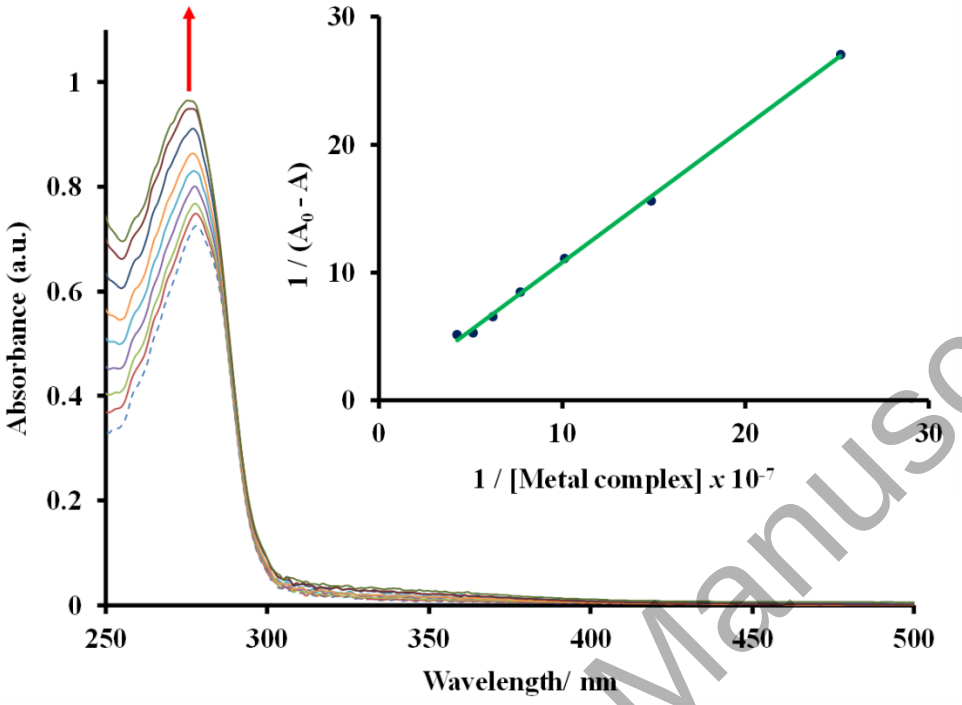

Figure 5: Fluorescence emission spectral profile depicting the titration between the metal complex **2** and BSA. Volumes of DNA solutions range from 0 to 34 µL.

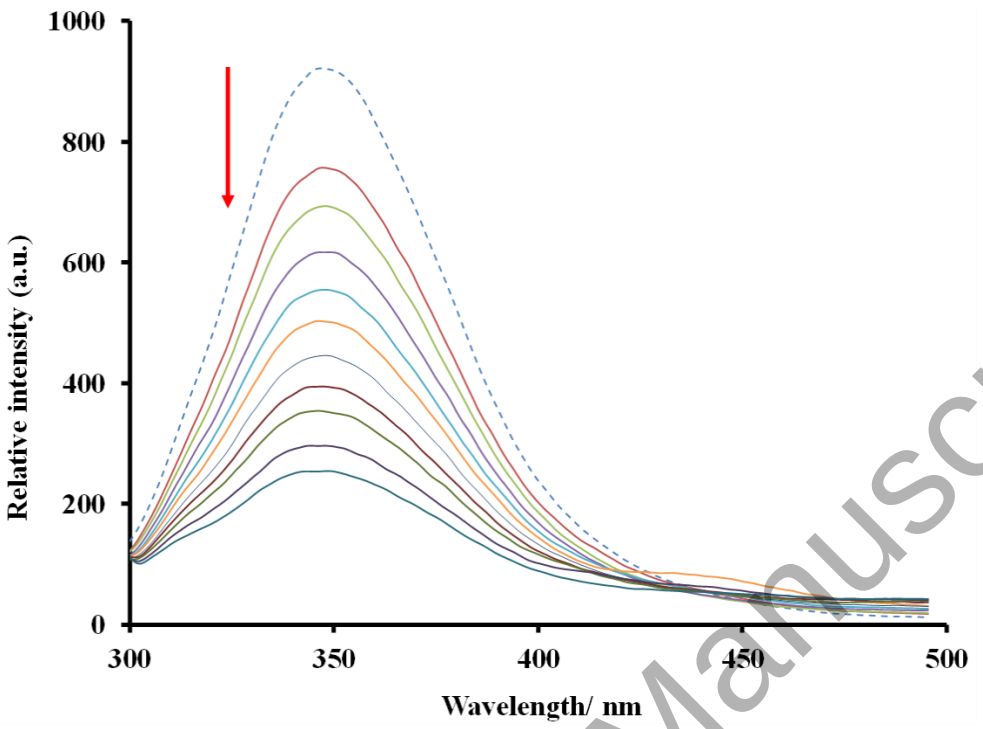

Figure 6: The plots of $\frac{Log\,[F_o - F]}{F}$ vs $Log\,[Q]$ for the metal complexes.

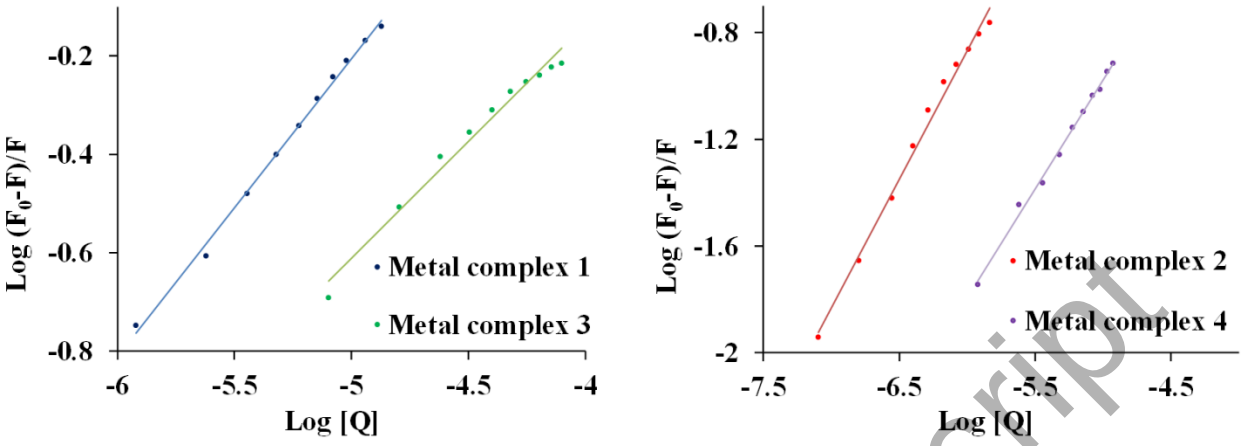

Table 1: *Antioxidant activities of **1** – **4** and Vitamin C against the DPPH and NO radicals as well as their corresponding intrinsic binding constants (K_b).*

Metal complex	DPPH Radical IC_{50} (μM)*	NO Radical IC_{50} (μM)*	K_b (M^{-1})
1	45	10	1.5×10^5
2	47	12	1.2×10^7
3	29	8	9×10^4
4	40	10	2×10^5
Vitamin C	141	210	-

**standard deviation is less than 8 % of mean values*

Table 2: *Stern-Volmer, quenching rate and intrinsic binding constants obtained of the composites comprised of BSA and the corresponding metal complexes.*

Metal complex	K_{SV} (M^{-1})	k_q (M^{-1} s^{-1})	K_b (M^{-1})
1	1.48×10^5	1.48×10^{13}	8.34×10^4
2	1.98×10^5	1.98×10^{13}	6.65×10^2
3	1.85×10^4	1.85×10^{12}	5.79×10^1
4	1.11×10^4	1.11×10^{12}	1.27×10^3

Table 3: *Cytotoxicity analysis of the metal complexes against the different cancer cells.*

Metal complexes	IC_{50} values against HCC70 cells	IC_{50} values against HeLa cells
1	88.20 ± 1.10 μM (R^2 = 0.9656)	17.42 ± 1.14 μM (R^2 = 0.9491)
2	Non-toxic	Non-toxic
3	44.07 ± 1.12 μM (R^2 = 0.9702)	16.59 ± 1.16 μM (R^2 = 0.9328)
4	39.37 ± 1.15 μM (R^2 = 0.9593)	26.13 ± 1.16 μM (R^2 = 0.9215)
5-FU	127.07 ± 8.61 μM (R^2 = 0.8667)	-
Paclitaxel	3.06 ± 1.11 nM (R^2 = 0.9595)	31.03 ± 1.15 nM (R^2 = 0.9760)